Commun. Comput. Phys.
doi: 10.4208/cicp.031110.080711s

Vol. **12**, No. 3, pp. 885-918
September 2012

Multi-Physics Analyses of Selected Civil Engineering Concrete Structures

J. Kruis*, T. Koudelka and T. Krejčí

Department of Mechanics, Faculty of Civil Engineering, Czech Technical University, Thákurova 7, Prague, 166 29, Czech Republic.

Received 3 November 2010; Accepted (in revised version) 8 July 2011

Available online 1 March 2012

Abstract. This paper summarizes suitable material models for creep and damage of concrete which are coupled with heat and moisture transfer. The fully coupled approach or the staggered coupling is assumed. Governing equations are spatially discretized by the finite element method and the temporal discretization is done by the generalized trapezoidal method. Systems of non-linear algebraic equations are solved by the Newton method. Development of an efficient and extensible computer code based on the C++ programming language is described. Finally, successful analyses of two real engineering problems are described.

AMS subject classifications: 74C10, 74F05, 74F10, 74R05, 74S05, 76R50, 80A20, 80M10

Key words: Coupled problems, heat and moisture transfer, creep, damage mechanics, hydro-thermo-mechanical analysis, efficient solvers, analysis of containment, watertightness of foundation slabs.

1 Introduction

Analyses of many engineering and scientific problems become more complicated in the course of time because the multiphysics approach is required in branches where the single physics was satisfactory several years ago. Civil engineering is not an exception which can be documented on coupled analyses used for very important and monumental structures. Usually the mechanical analysis coupled with heat and moisture transfer is considered. The multiphysics approach can be used because of large achievements in numerical methods and significant development of computers, especially the parallel computers.

*Corresponding author. *Email addresses:* jk@cml.fsv.cvut.cz (J. Kruis), koudelka@cml.fsv.cvut.cz (T. Koudelka), krejci@cml.fsv.cvut.cz (T. Krejčí)

From many multiphysics problems of civil engineering, this paper concentrates only on the coupled hydro-thermo-mechanical analysis of concrete structures. The paper describes selected material models for mechanical and transport processes, balance and governing equations, their approximation by the finite element method, efficient methods for time discretization and solvers of algebraic equations. Special attention is devoted to development of a computer code which has to be easily extensible and very efficient. At the end, some real world engineering problems solved by the authors during past five years are described.

Concrete represents a very specific material which requires multiphysics analysis because the mechanical behaviour depends strongly on distribution of moisture and temperature. In the past, moisture and temperature were assumed time independent or they were not taken into account at all. The coupled hydro-thermo-mechanical approach enables description of real conditions and the material and structural response is in accordance with experiments.

The classical mechanical analysis based on the finite element method defines two or three unknown displacements in nodes of the mesh with respect to the dimension of problem solved. Heat and moisture transfer can be described by models which define two or three unknown nodal values. The unknowns represent nodal temperature, moisture content, relative humidity or partial pressures. In the general three-dimensional case, the coupled analysis deals with six unknowns in each node of the mesh. It is clear that the requirements on computers grow rapidly with the growing number of nodes in the mesh.

The classical single processor implementation of coupled problems gives severe limits on finite element mesh. Unfortunately, the mesh has to take into account the shape of the structure solved as well as possible steep gradients of all unknown variables. Only two-dimensional or very simple three-dimensional problems can be treated on a single processor computer. On the other hand, parallel computers with several processors together with domain decomposition methods represent a very efficient tool which is able to deal with significantly larger problems and reasonably fine meshes. The domain decomposition methods were successfully applied in various problems in past twenty years [9,19–21,31,34,40].

Another possibility of efficient solution of complicated multiphysics problems is application of adaptive methods. It is known, that there are basically three types of adaptive methods connected with the finite element approach. The h-version changes the meshes while the degree of polynomials used for approximation on finite elements is constant. On the other hand, the p-version changes the degree of polynomials used while the finite element mesh is fixed. Finally, the most efficient hp-version combines the previous approaches, i.e. the mesh and the degree of polynomials are changed simultaneously [36]. Clearly, the hp-version is the most difficult version in the perspective of computer implementation but it saves significant number of degrees of freedom which leads to shorter computational time and smaller demands on computer memory [37].

The paper is organized as follows. Section 2 summarizes useful mechanical material

models for concrete which are applied in pure mechanical analyses and coupled analyses as well. Models of creep, isotropic and orthotropic damage are mentioned. Section 3 is devoted to models of heat and moisture transfer. Namely, Künzel and Kiessl's model is described. Section 4 deals with numerical methods for time discretization and the Newton method for solution of non-linear algebraic equations. Section 5 describes implementation of material models, numerical methods and solvers. Requirements on extensibility and performance efficiency are also taken into account. The last section 6 describes selected real engineering problems solved. The analysis of watertightness of a foundation slab and simulation of a reactor vessel are mentioned in detail.

2 Mechanical models

Concrete is heterogeneous material whose behaviour is very complex. Creep, shrinkage, thermal dilatancy, plasticity, damage and crack propagation are the most important phenomena which should be taken into account for concrete modelling. Usually, the models describe only one aspect of concrete behaviour and this leads to combination of several material models. Assuming small strains, the total strain can be additively decomposed into several parts

$$\boldsymbol{\varepsilon} = \boldsymbol{\varepsilon}_e + \boldsymbol{\varepsilon}_p + \boldsymbol{\varepsilon}_d + \boldsymbol{\varepsilon}_c + \boldsymbol{\varepsilon}_{sh} + \boldsymbol{\varepsilon}_t, \tag{2.1}$$

where $\boldsymbol{\varepsilon}$ denotes the total strain, $\boldsymbol{\varepsilon}_e$ denotes the elastic strain, $\boldsymbol{\varepsilon}_p$ stands for the plastic strain, $\boldsymbol{\varepsilon}_d$ stands for damage strain, $\boldsymbol{\varepsilon}_c$ is creep strain which contains also contributions caused by ageing, $\boldsymbol{\varepsilon}_{sh}$ denotes part of strain caused by shrinkage and $\boldsymbol{\varepsilon}_t$ is free thermal strain. The resulting stress $\boldsymbol{\sigma}$ can be expressed from the Hook's law of elasticity in the form

$$\boldsymbol{\sigma} = \boldsymbol{D}_e \boldsymbol{\varepsilon}_e, \tag{2.2}$$

where $\boldsymbol{D}_e$ is the elastic stiffness of material.

Following subsections summarize models based on small strains used for analyses of real concrete structures described in this paper. In the case of geometrical non-linearity, the additive strain decomposition is not acceptable and different approach has to be used (e.g. [26]). The models described can be applied to matured concrete while special models have to be used for very early ages [38].

2.1 Concrete creep, effect of moisture and temperature

When taking into account the effects included in equation (2.1), the creep strain is most influenced by the moisture and temperature distribution and their history. Therefore, the creep has to be coupled with the heat and moisture transfer in order to obtain close agreement between numerical simulation and experiments. There are special problems, e.g. analysis of containment and reactor vessels in nuclear power plants, watertightness of foundation slabs or long term behaviour of long-span bridges, where the creep of concrete plays a very important role.

The areas of application of coupled heat and moisture transfer models are much more extensive. They also include problems such as energy storage and recovery, geothermal storage, nuclear waste disposal, evaluating the safety of peculiar concrete structures, and many others. The magnitude of pore pressures and the loss of moisture caused by heating of concrete is of considerable concern for predicting the response of prestressed concrete reactor vessels to hypothetical core disruption accidents as well as the response of concrete structures to fire. When solving the latter problem, a suitable constitutive law is required to describe the time-dependent behaviour of a structure due to shrinkage and creep. Pore relative humidity and temperature influence the creep and shrinkage in two ways – directly, by varying the viscosity coefficients in a constitutive model, and indirectly, through the effect of the rate of hydration (ageing). Temperature and pore humidity have also the direct effect on the rate of creep. To this end, the most convenient representations of compliance $J(t,t')$ in terms of the Dirichlet-Prony series are considered

$$J(t,t') = \sum_{\mu=1}^{M} \frac{1}{D_\mu(t')} \left\{1 - \exp\left[y_\mu(t') - y_\mu(t)\right]\right\}, \tag{2.3}$$

where $y_\mu(t) = (t/\tau_\mu)^{q_\mu}$, $q_\mu \leq 1$ is a coefficient (usually $q_\mu = \frac{2}{3}$). The compliance function of a linear viscoelastic material represents the strain at time t due to a unit stress $\sigma = 1$ applied at time t'. A proper selection of retardation times τ_μ for $J(t,t')$ can be found in [2]. Functions D_μ are usually obtained by fitting the compliance functions (2.3) using the method of least squares (see, e.g., [13]).

2.1.1 B3 creep model

As the most popular, Bazant's B3 model with logarithmic-power law was used to describe concrete creep

$$J(t,t') = q_1 + q_2 Q(t,t') + q_3 \ln\left[1 + \left(\frac{t-t'}{\lambda_0}\right)^n\right] + q_4 \ln\left(\frac{t}{t'}\right), \tag{2.4}$$

where $J(t,t')$ is the compliance function at time t due to a unit stress $\sigma = 1$ applied at time t'. The material parameter q_1 is the instantaneous strain due to unit stress. The term with the coefficient q_2 represents the ageing viscoelastic compliance, q_3 non-ageing viscoelastic compliance and q_4 flow compliance. The coefficient λ_0 is almost equal to 1.0 and $Q(t,t')$ is a binomial integral. Detailed description of all coefficients can be found, e.g., in [3].

2.1.2 Moisture and temperature effect

Any model which has to describe concisely the behaviour of concrete structures exposed to temperature and moisture changes should cover three complex phenomena in concrete creep (solidification model [5]):

- The ageing of concrete, which is manifested by a significant decrease of creep with the age at loading is of two types:

  - Shorter-term chemical ageing, which ceases at room temperature after about a year and is caused by the fact that new solids are produced by the slowly advancing chemical reactions of cement hydration and deposit (in an essentially stress-free) on the walls of capillary pores.
  - Long-term non-chemical ageing, manifested by the fact that the decrease of creep with the age at loading continues unabated even for many years after the degree of hydration of cement ceased to grow.

- The drying creep effect, also called the stress-induced shrinkage or Picket effect, which is a transient effect consisting in the fact that the apparent creep during drying is much larger than the basic creep (i.e., creep at moisture saturation) while the creep after drying (i.e., after reaching thermodynamical equilibrium with a reduced environmental humidity) is much smaller than basic creep. It consists of an apparent mechanism consisting of an apparent additional creep due to microcracking and a true mechanism that resides in the nanostructure.
- The transitional creep, which represents a transient increase of creep after a temperature change, both heating and cooling. In the case of cooling, the transient increase is of the opposite sign than the final change in creep rate after a steady-state lower temperature has been regained. Like the drying creep effect, this effect has two analogous mechanisms [5]:

  - An apparent macroscopic mechanism, due to thermally induced microcracking and similar to drying creep.
  - A nanoscale mechanism due to a change in the level of microprestress caused by a change of chemical potential of nanopore water with a temperature change.

The effect of temperature on concrete creep is twofold, generated by two different mechanisms:

- A temperature increase accelerates the bond breakages and restorations causing creep, and thus increases the creep rate.
- The higher the temperature, the faster is the chemical process of cement hydration and thus the ageing of concrete, which reduces the creep rate.

Usually the former effect prevails and then the overall effect of temperature rise in an increase of creep. The special time quantities are applied into creep model:

- Reduced time t_r characterizing the changes in the rate of bond breakages and restoration on the microstructural level

$$t_r(t) = \int_0^t \psi(t')\mathrm{d}t' \leq t, \tag{2.5}$$

where

$$\psi(t)=\psi_T(t)\psi_\varphi(t), \tag{2.6}$$

$$\psi_T(t)=\exp\left\{\frac{Q_v}{R}\left(\frac{1}{T_0}-\frac{1}{T}\right)\right\}, \tag{2.7}$$

$$\psi_\varphi(t)=\alpha_\varphi+(1-\alpha_\varphi)\varphi^2(t), \tag{2.8}$$

where T is the absolute temperature, T_0 is the reference temperature, φ is the relative humidity in the pores of cement paste, R is the gas constant, Q_v is the activation energy for the viscous processes and α_φ is a material parameter that has to be determined experimentally. With respect to a large set of experiments, Bazant determined the following parameters $T_0=294$ K, $Q_v/R=5000$ K and $\alpha_\varphi=0.1$.

- Equivalent time t_e (equivalent hydration period or maturity), which indirectly characterizes the degree of hydration ($t_e\geq t$)

$$t_e(t)=\int_0^t \beta(t')\mathrm{d}t', \tag{2.9}$$

where

$$\beta(t)=\beta_T(t)\beta_\varphi(t), \tag{2.10}$$

$$\beta_T(t)=\exp\left\{\frac{Q_h}{R}\left(\frac{1}{T_0}-\frac{1}{T}\right)\right\}, \tag{2.11}$$

$$\beta_\varphi(t)=\{1+[a_\varphi-a_\varphi\varphi(t)]^4\}^{-1}, \tag{2.12}$$

where Q_h is the activation energy, $Q_h/R=2700$ K and $a_\varphi=5$.

Moisture changes have the similar effect in ageing of concrete [5]. The rate of hydration and creep decrease with decreasing relative humidity φ and when φ approaches 0.3, the rate of ageing is almost zero.

The effect of temperature and humidity changes (structural thermal expansion and shrinkage) at zero stress can be expressed in strain rates:

- thermal expansion rate

$$\dot{\boldsymbol{\varepsilon}}_t=\boldsymbol{\alpha}\dot{T} \quad\Rightarrow\quad \Delta\boldsymbol{\varepsilon}_t=\boldsymbol{\alpha}\dot{T}\Delta t=\boldsymbol{\alpha}\Delta T, \tag{2.13}$$

- drying shrinkage rate

$$\dot{\boldsymbol{\varepsilon}}_{sh}=\boldsymbol{k}\dot{\varphi} \quad\Rightarrow\quad \Delta\boldsymbol{\varepsilon}_{sh}=\boldsymbol{k}\dot{\varphi}\Delta t=\boldsymbol{k}\Delta\varphi, \tag{2.14}$$

where $\boldsymbol{k}=\{k_{11},k_{22},k_{33},k_{23},k_{31},k_{12}\}^{\mathrm{T}}$ is the incremental shrinkage coefficient vector, which depends on φ, T and t_e, and $\boldsymbol{\alpha}=\{\alpha_{11},\alpha_{22},\alpha_{33},\alpha_{23},\alpha_{31},\alpha_{12}\}^{\mathrm{T}}$ is the thermal expansion coefficient vector.

Providing the shrinkage and thermal expansion are independent of stress, they assume the form

$$\boldsymbol{k}=\varepsilon_{sh}^{0}\psi\boldsymbol{m},\qquad \boldsymbol{\alpha}=\alpha^{0}\boldsymbol{m},\qquad \boldsymbol{m}=\{1,1,1,0,0,0\}^{\mathrm{T}}, \tag{2.15}$$

where $(-\varepsilon_{sh}^{0})=0.0002\div0.001$ and α^{0} are empirical constants, and $(-\psi)=E(t')/E(t_e)3\varphi^2$ for $0.4\leq\varphi\leq0.98$.

In the presence of stress, the shrinkage and thermal expansion coefficient vectors are approximated as linear functions of the stress vector [4], $\boldsymbol{\sigma}=\{\sigma_{11},\sigma_{22},\sigma_{33},\sigma_{23},\sigma_{31},\sigma_{12}\}^{\mathrm{T}}$ as

$$\boldsymbol{k}=\varepsilon_{sh}^{0}\psi(\boldsymbol{m}+r\boldsymbol{\sigma}\,\mathrm{sign}(\dot{H})),\qquad \boldsymbol{\alpha}=\alpha^{0}(\boldsymbol{m}+\rho\boldsymbol{\sigma}\,\mathrm{sign}(\dot{H})), \tag{2.16}$$

where $\dot{H}=\dot{\varphi}+c\dot{T}$ (c being a non-negative constant). Empirical coefficients normally attain the values $r=(0.1\div0.6)/f_t'$ (MPa^{-1}), $\rho=(1\div2)/f_t'$ (MPa^{-1}), where f_t' is the tensile strength. In [2], Eq. (2.16) are simplified by considering $c\to0$ in case of $\boldsymbol{k}$, to get $\mathrm{sign}(\dot{H})=\mathrm{sign}(\dot{\varphi})$, and by setting $c\to\infty$ in case of $\boldsymbol{\alpha}$, thus yielding $\mathrm{sign}(\dot{H})=\mathrm{sign}(\dot{T})$. A general linear dependence (2.16) would also include terms proportional to $\sigma_{\mathrm{mean}}=\boldsymbol{\sigma}^{\mathrm{T}}\boldsymbol{m}/3$, which, however, seem to be negligible.

Generalization into 3D and including incremental form of shrinkage $\Delta\boldsymbol{\varepsilon}_{\mathrm{sh}}=\boldsymbol{k}\Delta\varphi$ and thermal dilatation $\Delta\boldsymbol{\varepsilon}_t=\boldsymbol{\alpha}\Delta T$, the incremental constitutive equation based on the Dirichlet-Prony series is obtained

$$\Delta\boldsymbol{\sigma}=\widehat{E}_i\widehat{\boldsymbol{D}}\left(\Delta\boldsymbol{\varepsilon}-\boldsymbol{k}\Delta\varphi-\boldsymbol{\alpha}\Delta T-\Delta\boldsymbol{\varepsilon}_{\mathrm{c}}-\Delta\boldsymbol{\varepsilon}_{\mathrm{d}}\right), \tag{2.17}$$

where

$$\widehat{E}_i=\sum_{\mu=1}^{M}\frac{\bar{E}_\mu}{\Delta y_\mu}\left(1-e^{-\Delta y_\mu}\right),\qquad \text{with}\quad \bar{E}_\mu=\frac{1}{D_\mu}, \tag{2.18}$$

$$\widehat{\boldsymbol{C}}=\widehat{\boldsymbol{D}}^{-1}=\begin{pmatrix} 1 & -\nu & -\nu & 0 & 0 & 0\\ & 1 & -\nu & 0 & 0 & 0\\ & & 1 & 0 & 0 & 0\\ & & & 2(1+\nu) & 0 & 0\\ & & & & 2(1+\nu) & 0\\ & & & & & 2(1+\nu) \end{pmatrix}. \tag{2.19}$$

2.2 Scalar isotropic damage model

Concrete belongs to quasi-brittle materials. In such materials, exceeding of a certain level of strains leads to evolution of defects such as microcracks and microvoids. If the evolution of strains continues, the growth of defects localizes to some of them while evolution of the rest stops. The process is called as localization of inelastic strains. It can be described by a variety of models depending on the concept of yielding.

The scalar isotropic damage model is one of the simplest models of continuum damage mechanics. More details about the model can be found in [24] and [33]. The damage

models consist in concepts of virgin, damaged and pseudo-undamaged states of material. The material is assumed to be at virgin state when no defects are present which corresponds to elastic state. Considering the one-dimensional case, the area of the cross-section of a bar element is denoted by A at the virgin state. The bar element is subjected to increasing uniaxial stress. Evolution of defects starts at a certain level of deformation. Let the area of these defects be denoted by A_d. In the damaged state, the nominal stress σ is assumed acting on the original cross-section area A while in the pseudo-undamaged state the effective stress $\tilde{\sigma}$ acts on the undamaged area $\tilde{A}=A-A_d$. The equilibrium condition on the bar element can be written in the form

$$\sigma A=\tilde{\sigma}\tilde{A} \tag{2.20}$$

and dimensionless damage parameter ω can be defined

$$\omega=\frac{A_d}{A}. \tag{2.21}$$

Using Eqs. (2.20) and (2.21), the stress-strain relation for the one-dimensional case can be written

$$\sigma=(1-\omega)E\bar{\varepsilon}, \tag{2.22}$$

where $\bar{\varepsilon}$ represents strain without irreversible strains in the form

$$\bar{\varepsilon}=\varepsilon-\varepsilon_p-\varepsilon_c-\varepsilon_{sh}-\varepsilon_t \tag{2.23}$$

and E is the Young modulus of elasticity. Eq. (2.22) can be rewritten to the form

$$\sigma=E(\bar{\varepsilon}-\varepsilon_d)=E\varepsilon_e, \tag{2.24}$$

where

$$\varepsilon_d=\omega\bar{\varepsilon}. \tag{2.25}$$

Additionally, the evolution law for damage parameter ω has to be established and it depends on the type of the modelled material. In reference [28], the evolution law suitable for concrete was proposed in the form

$$\omega=\frac{a(\bar{\varepsilon}-\bar{\varepsilon}_0)^b}{1+a(\bar{\varepsilon}-\bar{\varepsilon}_0)^b}, \tag{2.26}$$

where $\bar{\varepsilon}_0$ is the strain threshold, a and b are material parameters controlling the peak value and slope of the softening branch. The damage evolves after the strains exceed the limit value of $\bar{\varepsilon}_0$.

It is known, [24], that damage models are mesh sensitive. It is connected with the dissipated energy which depends on the characteristic size of a damaged element and it leads to physically unrealistic results. Dissipated energy tends to zero with decreasing

characteristic size of the element. The so-called method of the variable softening modulus was developed, [30], in order to avoid the spurious mesh dependency. The method consists in involving of the characteristic element length into the damage evolution law. Assuming the one-dimensional case, the stress can be expressed in the form

$$\sigma = f_t \exp\left(-\frac{w_{cr}}{w_{cr0}}\right), \tag{2.27}$$

where f_t is the tensile strength in [Pa], w_{cr} is the crack opening in [m] and w_{cr0} is the material parameter controlling the initial slope of the softening branch in [m]. The crack opening can be smeared over the element using the following equation

$$\bar{\varepsilon} - \varepsilon_e = \frac{w_{cr}}{h}, \tag{2.28}$$

where h is the characteristic element length. When combining Eqs. (2.22), (2.28) and (2.27), the resulting non-linear equation for the damage parameter ω yields

$$(1-\omega) E \bar{\varepsilon} = f_t \exp\left(-\frac{\omega h \bar{\varepsilon}}{w_{cr0}}\right). \tag{2.29}$$

In the general three-dimensional case, the stress-strain relation can be obtained similarly in the form

$$\boldsymbol{\sigma} = (1-\omega)\boldsymbol{D}_e \bar{\boldsymbol{\varepsilon}}. \tag{2.30}$$

The damage parameter ω is computed with help of the evolution law similar to the one-dimensional case where the strain $\bar{\varepsilon}$ has to be substituted by equivalent strain κ. There are many definitions of the equivalent strain κ but in the case of concrete modelling, the most used definition is the Mazars' norm [27] which has the form

$$\kappa = \sqrt{\langle \bar{\varepsilon}_\alpha \rangle \langle \bar{\varepsilon}_\alpha \rangle}, \tag{2.31}$$

where $\bar{\varepsilon}_\alpha$ denotes the principal values of the strain tensor $\bar{\boldsymbol{\varepsilon}}$ and the symbol $\langle\rangle$ denotes selection of positive components (McAulley brackets).

2.3 Orthotropic damage model

The main drawback of the scalar isotropic damage model is that it uses only one damage parameter for all principle directions regardless of tension or compression. Once the damage parameter caused by exceeding limit strain in one principle direction evolves, it reduces stiffness in all remaining principle directions even though they should not be influenced. This drawback is not significant in the case of the one-dimensional stress state such as pure bending but it becomes more important especially for the three-dimensional stress state.

That led to development of the more advanced damage model which can describe better the 3D problems. In reference [28], the authors proposed general anisotropic model for concrete which contains nine material parameters. The laboratory measurements of the required material parameters has to be performed but it caused difficulties for certain cases. Additionally, the model required a significant number of internal variables that have to be stored. These difficulties led to development of a simplified version of the model which is based on six material parameters – three for tension and another three parameters for compression.

The model is based on the following stress-strain relation

$$\sigma_\alpha = \left(1-H(\bar{\varepsilon}_\alpha)D_\alpha^{(t)}-H(-\bar{\varepsilon}_\alpha)D_\alpha^{(c)}\right)\left[\left(K-\frac{2}{3}G\right)\bar{\varepsilon}_v+2G\bar{\varepsilon}_\alpha\right], \tag{2.32}$$

where the subscript α stands for the index of principle components of the given quantity. The model defines two sets of damage parameters $D_\alpha^{(t)}$ and $D_\alpha^{(c)}$ for tension and compression, respectively. In the equation (2.32), the symbol $H()$ denotes the Heaviside function, K is the bulk modulus, G is the shear modulus and $\bar{\varepsilon}_v$ stands for volumetric strain.

There are many evolution laws that can be used for $D_\alpha^{(t)}$ and $D_\alpha^{(c)}$ description. In our problems, the two evolution laws for the damage parameters are used similar to the laws used in the scalar isotropic damage model. The first law gives better results for compression but the determination of the material parameters is more complicated. It can be written in the form

$$D_\alpha^{(\beta)} = \frac{A^{(\beta)}\left(|\bar{\varepsilon}_\alpha^{(\beta)}|-\bar{\varepsilon}_0^{(\beta)}\right)^{B^{(\beta)}}}{1+A^{(\beta)}\left(|\bar{\varepsilon}_\alpha^{(\beta)}|-\bar{\varepsilon}_0^{(\beta)}\right)^{B^{(\beta)}}}, \tag{2.33}$$

where the superscript (β) represents indices t or c which are used for tension and compression. $A^{(\beta)}$, $B^{(\beta)}$ and $\bar{\varepsilon}_0^{(\beta)}$ are material parameters with the same meaning as in the similar law defined by (2.26). The second law involves correction of the dissipated energy with respect to the size of elements and it describes tension better. It is defined by the non-linear equation (2.34) which can be solved using the Newton method

$$\left(1-D_\alpha^{(\beta)}\right)E|\bar{\varepsilon}_\alpha^{(\beta)}| = f_\beta \exp\left(-\frac{D_\alpha^{(\beta)}h|\bar{\varepsilon}_\alpha^{(\beta)}|}{w_{cr0}^{(\beta)}}\right). \tag{2.34}$$

In the above equation, f_β represents the tensile or compressive strength and $w_{cr0}^{(\beta)}$ controls the initial slope of the softening branches. More details about the implemented models can be found in [16–18].

3 Heat and moisture transfer

Transport of heat and moisture in porous medium can be assumed by convection, diffusion or their combination. In all cases, three types of equations have to be solved. The transport equations express fluxes with respect to gradients of unknown variables. The constitutive equations define relationships between unknown variables and internal variables. As an example can serve the retention curves, sorption isotherms, etc. Finally, the third set of equations contains the balance (conservation) equations. Gradual substitution of the constitutive equations to the transport equations and then to the balance equations leads to the governing equations. The governing equations are partial differential equations and they have to be solved numerically. After spatial discretization of governing equations using the finite element method and after temporal discretization by the generalized trapezoidal method, the system of non-symmetric and non-linear algebraic equations is obtained.

One of the most popular models is summarized in this paper. It is the Künzel and Kiessl's phenomenological model [23] based on the diffusion theory. This model is suitable for numerical simulations of building structures under common climatic conditions. Other models and description of climatic conditions can be found in references [6, 10, 14, 15, 25, 29].

3.1 Künzel and Kiessl's coupled heat and moisture transfer approach

The model introduces two unknowns in a material point, relative humidity φ [-] and temperature T [K]. The model divides overhygroscopic region into two subranges – capillary water region and supersaturated region, where different conditions for water and water vapour transport are considered. For the description of simultaneous water and water vapour transport, the relative humidity φ is chosen as the only moisture potential for both hygroscopic and overhygroscopic range. This model uses certain simplifications. Nevertheless, proposed model describes all substantial phenomena and the predicted results comply well with experimentally obtained data, which is the main advantage of the model together with easy and quick determination of the material properties measured in a laboratory.

3.1.1 Transport equations

Künzel proposed that the moisture transport mechanisms relevant to numerical analysis in the field of building physics are just water vapour diffusion and liquid transport [23]. Vapour diffusion is the most important in large pores, whereas liquid transport takes place on pore surfaces and in small capillaries.

Vapour diffusion in porous media is described in the model by the Fick's diffusion and effusion in the form

$$J_v = -\delta_p \nabla p = -\frac{\delta}{\mu} \nabla p, \tag{3.1}$$

where J_v is the water vapour flux, δ_p [kg m^{-1} s^{-1} Pa^{-1}] is the vapour permeability of the porous material, p denotes vapour pressure [Pa], the vapour diffusion resistance number μ is a material property and δ [kg m^{-1} s^{-1} Pa^{-1}] is the vapour diffusion coefficient in the air.

The liquid transport mechanism includes liquid flow in the absorbed layer (surface diffusion) and in the water filled capillaries (capillary transport). The driving potential in both cases is capillary pressure (suction stress) or relative humidity φ. The flux of liquid water is described by

$$J_w = -D_\varphi \nabla \varphi, \tag{3.2}$$

where the liquid conductivity D_φ [kg m s^{-1}] is the product of the liquid diffusivity D_w [m^2 s^{-1}] and the derivative of water retention function $D_\varphi = D_w \cdot \mathrm{d}w/\mathrm{d}\varphi$.

The heat flux is proportional to the thermal conductivity of the moist porous material and the temperature gradient (Fourier's law)

$$q = -\lambda \nabla T, \tag{3.3}$$

where λ [W m^{-1} K^{-1}] is the thermal conductivity of the moist material. The enthalpy flows through moisture movement and phase transition is taken into account in the form of source terms in the heat balance equation.

3.1.2 Balance equations

The heat and moisture balance equations are closely coupled because the moisture content depends on the total enthalpy and thermal conductivity while the temperature depends on moisture flow. The resulting set of differential equations for the description of simultaneous heat and moisture transfer, expressed in terms of temperature T and relative humidity φ, have the form of partial differential equations defined on a domain Ω

$$\frac{\mathrm{d}w}{\mathrm{d}\varphi}\frac{\partial \varphi}{\partial t} = \nabla^{\mathrm{T}}\left(D_\varphi \nabla \varphi + \delta_p \nabla(\varphi p_{\mathrm{sat}})\right), \qquad \boldsymbol{x} \in \Omega, \tag{3.4}$$

$$\left(\rho C + \frac{\mathrm{d}H_w}{\mathrm{d}T}\right)\frac{\partial T}{\partial t} = \nabla^{\mathrm{T}}\left(\lambda\, \nabla T\right) + h_v \nabla^{\mathrm{T}}\left(\delta_p \nabla(\varphi p_{\mathrm{sat}})\right), \qquad \boldsymbol{x} \in \Omega, \tag{3.5}$$

where H_w [J m^{-3}] is the enthalpy of the material moisture, w [kg m^{-3}] is the water content of the material, h_v [J kg^{-1}] is the evaporation enthalpy of the water, p_{sat} [Pa] is the water vapour saturation pressure, ρ [kg m^{-3}] is the material density, C [J kg^{-1} K^{-1}] is the specific heat capacity and t [s] denotes time. Boundary of the domain Ω is split into parts Γ_T, Γ_φ, Γ_{qpT}, $\Gamma_{Jp\varphi}$, Γ_{qcT} and $\Gamma_{Jc\varphi}$. The parts Γ_T, Γ_{qpT} and Γ_{qcT} are disjoint and their union is the whole boundary Γ. The same is valid for the parts Γ_φ, $\Gamma_{Jp\varphi}$ and $\Gamma_{Jc\varphi}$. The heat fluxes are prescribed on the part $\Gamma_q = \Gamma_{qpT} \bigcup \Gamma_{qcT}$ and the moisture fluxes are prescribed on the part $\Gamma_J = \Gamma_{Jp\varphi} \bigcup \Gamma_{Jc\varphi}$.

3.1.3 Initial and Boundary conditions

The system of equations (3.4) and (3.5) are accompanied with three types of boundary conditions:

- Dirichlet boundary conditions

$$T(\boldsymbol{x},t)=\overline{T}(\boldsymbol{x},t), \qquad \boldsymbol{x}\in\Gamma_T, \tag{3.6}$$
$$\varphi(\boldsymbol{x},t)=\overline{\varphi}(\boldsymbol{x},t), \qquad \boldsymbol{x}\in\Gamma_\varphi, \tag{3.7}$$

- Neumann boundary conditions

$$\boldsymbol{q}(\boldsymbol{x},t)=\overline{\boldsymbol{q}}(\boldsymbol{x},t), \qquad \boldsymbol{x}\in\Gamma_{qpT}, \tag{3.8}$$
$$\boldsymbol{J}(\boldsymbol{x},t)=\overline{\boldsymbol{J}}(\boldsymbol{x},t), \qquad \boldsymbol{x}\in\Gamma_{Jp\varphi}, \tag{3.9}$$

- Cauchy boundary conditions

$$\boldsymbol{q}(\boldsymbol{x},t)=\beta_T(T(\boldsymbol{x},t)-T_\infty(\boldsymbol{x},t)), \qquad \boldsymbol{x}\in\Gamma_{qcT}, \tag{3.10}$$
$$\boldsymbol{J}(\boldsymbol{x},t)=\beta_\varphi(p(\boldsymbol{x},t)-p_\infty(\boldsymbol{x},t)), \qquad \boldsymbol{x}\in\Gamma_{Jc\varphi}, \tag{3.11}$$

where $\overline{T}(\boldsymbol{x},t)$ is the prescribed temperature, $\overline{\varphi}(\boldsymbol{x},t)$ is the prescribed relative humidity, $\overline{\boldsymbol{q}}(\boldsymbol{x},t)$ is the prescribed heat flux, $\overline{\boldsymbol{J}}(\boldsymbol{x},t)$ is the prescribed moisture flux, β_T [W m^{-2} K^{-1}] and β_φ [kg s^{-1} Pa^{-1}] are the heat and mass transfer coefficient, T_∞ is the ambient temperature and p_∞ is the ambient water vapour pressure. Besides the boundary conditions, the initial conditions are prescribed, i.e.

$$T(\boldsymbol{x},0)=T_0(\boldsymbol{x}), \qquad \boldsymbol{x}\in\Omega, \tag{3.12}$$
$$\varphi(\boldsymbol{x},0)=\varphi_0(\boldsymbol{x}), \qquad \boldsymbol{x}\in\Omega, \tag{3.13}$$

where $T_0(\boldsymbol{x})$ denotes the initial temperature and $\varphi_0(\boldsymbol{x})$ denotes the initial relative humidity.

3.1.4 Discretization of the differential equations

The finite element method is used for spatial discretization of the partial differential equations (3.4) and (3.5). The weighted residual statement is applied to the mass balance equation assuming $\delta T=0$ on Γ_T and $\delta\varphi=0$ on Γ_φ

$$\int_\Omega \delta\varphi\Big(\frac{\mathrm{d}w}{\mathrm{d}\varphi}\frac{\partial\varphi}{\partial t}-\nabla^{\mathrm{T}}\big(D_\varphi\nabla\varphi+\delta_p\nabla(\varphi p_{\mathrm{sat}})\big)\Big)\mathrm{d}\Omega=0 \tag{3.14}$$

and also to the energy balance equation

$$\int_\Omega \delta T\Big(\big(\rho C+\frac{\mathrm{d}H_w}{\mathrm{d}T}\big)\frac{\partial T}{\partial t}-\nabla^{\mathrm{T}}\big(\lambda\,\nabla T\big)-h_v\nabla^{\mathrm{T}}\big(\delta_p\nabla(\varphi p_{\mathrm{sat}})\big)\Big)\mathrm{d}\Omega=0. \tag{3.15}$$

Applying Green's theorem the weak formulation for the mass transfer yields

$$\int_\Omega \delta\varphi\Big(\frac{\mathrm{d}w}{\mathrm{d}\varphi}\frac{\partial\varphi}{\partial t}\Big)\mathrm{d}\Omega+\int_\Omega \nabla(\delta\varphi)\Big(D_w\frac{\mathrm{d}w}{\mathrm{d}\varphi}+\delta_p p_{\mathrm{sat}}\Big)\nabla\varphi\mathrm{d}\Omega+\int_\Omega \nabla(\delta\varphi)\Big(\delta_p\varphi\frac{\mathrm{d}p_{\mathrm{sat}}}{\mathrm{d}T}\Big)\nabla T\mathrm{d}\Omega$$
$$-\int_{\Gamma_J}\delta\varphi\Big(D_w\frac{\mathrm{d}w}{\mathrm{d}\varphi}+\delta_p p_{\mathrm{sat}}\Big)\frac{\partial\varphi}{\partial\boldsymbol{n}}\mathrm{d}\Gamma-\int_{\Gamma_q}\delta\varphi\Big(\delta_p\varphi\frac{\mathrm{d}p_{\mathrm{sat}}}{\mathrm{d}T}\Big)\frac{\partial T}{\partial\boldsymbol{n}}\mathrm{d}\Gamma=0 \tag{3.16}$$

and the weak formulation for heat transfer

$$\int_\Omega \delta T\Big(\rho C+\frac{\mathrm{d}H_w}{\mathrm{d}T}\Big)\frac{\partial T}{\partial t}\mathrm{d}\Omega+\int_\Omega \nabla(\delta T)\Big(\lambda+h_v\delta_p\varphi\frac{\mathrm{d}p_{\mathrm{sat}}}{\mathrm{d}T}\Big)\nabla T\mathrm{d}\Omega$$
$$+\int_\Omega \nabla(\delta T)\Big(h_v\delta_p p_{\mathrm{sat}}\Big)\nabla\varphi\mathrm{d}\Omega-\int_{\Gamma_J}\delta T\Big(h_v\delta_p p_{\mathrm{sat}}\Big)\frac{\partial\varphi}{\partial\boldsymbol{n}}\mathrm{d}\Gamma$$
$$-\int_{\Gamma_q}\delta T\Big(\lambda+h_v\delta_p\varphi\frac{\mathrm{d}p_{\mathrm{sat}}}{\mathrm{d}T}\Big)\frac{\partial T}{\partial\boldsymbol{n}}\mathrm{d}\Gamma=0. \tag{3.17}$$

In the finite element method, the temperature T and relative humidity φ are approximated in the form

$$T=\boldsymbol{N}(\boldsymbol{x})\boldsymbol{d}_T,\qquad \varphi=\boldsymbol{N}(\boldsymbol{x})\boldsymbol{d}_\varphi \tag{3.18}$$

and the gradients of temperature and relative humidity are also needed

$$\nabla T=\boldsymbol{B}(\boldsymbol{x})\boldsymbol{d}_T,\qquad \nabla\varphi=\boldsymbol{B}(\boldsymbol{x})\boldsymbol{d}_\varphi. \tag{3.19}$$

In the previous equations, $\boldsymbol{N}(\boldsymbol{x})$ denotes the matrix of approximation functions, $\boldsymbol{B}(\boldsymbol{x})$ is the matrix of their derivatives, $\boldsymbol{d}_T$ denotes the vector of nodal temperatures and $\boldsymbol{d}_\varphi$ denotes the vector of nodal relative humidities. Using approximations (3.18) and (3.19) in Eqs. (3.16) and (3.17), a set of the first order differential equations is obtained in the matrix form

$$\begin{pmatrix}\boldsymbol{K}_{\varphi\varphi} & \boldsymbol{K}_{\varphi T}\\ \boldsymbol{K}_{T\varphi} & \boldsymbol{K}_{TT}\end{pmatrix}\begin{pmatrix}\boldsymbol{d}_\varphi\\ \boldsymbol{d}_T\end{pmatrix}+\begin{pmatrix}\boldsymbol{C}_{\varphi\varphi} & \boldsymbol{C}_{\varphi T}\\ \boldsymbol{C}_{T\varphi} & \boldsymbol{C}_{TT}\end{pmatrix}\begin{pmatrix}\dot{\boldsymbol{d}}_\varphi\\ \dot{\boldsymbol{d}}_T\end{pmatrix}=\begin{pmatrix}\boldsymbol{J}_\varphi\\ \boldsymbol{q}_T\end{pmatrix}. \tag{3.20}$$

The matrices $\boldsymbol{K}_{\varphi\varphi}$, $\boldsymbol{K}_{\varphi T}$, $\boldsymbol{K}_{T\varphi}$ and $\boldsymbol{K}_{TT}$ create the conductivity matrix of the problem and they have the form

$$\boldsymbol{K}_{\varphi\varphi}=\int_\Omega \boldsymbol{B}^T\boldsymbol{D}_{\varphi\varphi}\boldsymbol{B}\mathrm{d}\Omega,\qquad \boldsymbol{K}_{\varphi T}=\int_\Omega \boldsymbol{B}^T\boldsymbol{D}_{\varphi T}\boldsymbol{B}\mathrm{d}\Omega, \tag{3.21}$$

$$\boldsymbol{K}_{T\varphi}=\int_\Omega \boldsymbol{B}^T\boldsymbol{D}_{T\varphi}\boldsymbol{B}\mathrm{d}\Omega,\qquad \boldsymbol{K}_{TT}=\int_\Omega \boldsymbol{B}^T\boldsymbol{D}_{TT}\boldsymbol{B}\mathrm{d}\Omega, \tag{3.22}$$

where the conductivity matrices of material $\boldsymbol{D}_{\varphi\varphi}$, $\boldsymbol{D}_{\varphi T}$, $\boldsymbol{D}_{T\varphi}$ and $\boldsymbol{D}_{TT}$ are diagonal matrices and the diagonal entries are equal to appropriate conductivities

$$k_{\varphi\varphi}=D_w\frac{\mathrm{d}w}{\mathrm{d}\varphi}+\delta_p p_{\mathrm{sat}},\qquad k_{\varphi T}=\delta_p\varphi\frac{\mathrm{d}p_{\mathrm{sat}}}{\mathrm{d}T}, \tag{3.23}$$

$$k_{T\varphi}=h_v\delta_p p_{\mathrm{sat}},\qquad k_{TT}=\lambda+h_v\delta_p\varphi\frac{\mathrm{d}p_{\mathrm{sat}}}{\mathrm{d}T}. \tag{3.24}$$

The matrices $\boldsymbol{C}_{\varphi\varphi}$, $\boldsymbol{C}_{\varphi T}$, $\boldsymbol{C}_{T\varphi}$ and $\boldsymbol{C}_{TT}$ create the capacity matrix of the problem and they have the form

$$\boldsymbol{C}_{\varphi\varphi}=\int_\Omega \boldsymbol{N}^T\boldsymbol{H}_{\varphi\varphi}\boldsymbol{N}\mathrm{d}\Omega, \qquad \boldsymbol{C}_{\varphi T}=\int_\Omega \boldsymbol{N}^T\boldsymbol{H}_{\varphi T}\boldsymbol{N}\mathrm{d}\Omega, \tag{3.25}$$

$$\boldsymbol{C}_{T\varphi}=\int_\Omega \boldsymbol{N}^T\boldsymbol{H}_{T\varphi}\boldsymbol{N}\mathrm{d}\Omega, \qquad \boldsymbol{C}_{TT}=\int_\Omega \boldsymbol{N}^T\boldsymbol{H}_{TT}\boldsymbol{N}\mathrm{d}\Omega, \tag{3.26}$$

where capacity matrices of material $\boldsymbol{H}_{\varphi\varphi}$, $\boldsymbol{H}_{\varphi T}$, $\boldsymbol{H}_{T\varphi}$ and $\boldsymbol{H}_{TT}$ are diagonal matrices and the diagonal entries are equal to appropriate capacities

$$c_{\varphi\varphi}=\frac{\mathrm{d}w}{\mathrm{d}\varphi}, \qquad c_{\varphi T}=0, \tag{3.27}$$

$$c_{T\varphi}=0, \qquad c_{TT}=\rho C+\frac{\mathrm{d}H_w}{\mathrm{d}T}. \tag{3.28}$$

The vectors $\boldsymbol{J}_\varphi$ and $\boldsymbol{q}_T$ contain prescribed nodal fluxes and have the form

$$\boldsymbol{J}_\varphi=\int_{\Gamma_J}\boldsymbol{N}^T\overline{J}_\varphi\mathrm{d}\Gamma, \qquad \boldsymbol{q}_T=\int_{\Gamma_q}\boldsymbol{N}^T\overline{q}_T\mathrm{d}\Gamma, \tag{3.29}$$

where $\overline{J}_\varphi$ denotes the mass boundary fluxes and $\overline{q}_T$ denotes the heat boundary fluxes.

4 Numerical solution

From the numerical point of view, coupled problems are described by balance equations which have the form of partial differential equations. The exact solution cannot be obtained with respect to non-linearities hidden in the material models. Another obstacle is caused by very general domains which are solved in real engineering problems. Therefore, numerical methods have to be used.

The spatial discretization of the balance equations is done by the finite element method [7] and a system of ordinary differential equations with time variables is obtained. In the case of hydro-thermo-mechanical problem, the system may have the form

$$\begin{aligned}&\begin{pmatrix}\boldsymbol{C}_{uu}&\boldsymbol{C}_{uT}&\boldsymbol{C}_{u\varphi}\\ \boldsymbol{C}_{Tu}&\boldsymbol{C}_{TT}&\boldsymbol{C}_{T\varphi}\\ \boldsymbol{C}_{\varphi u}&\boldsymbol{C}_{\varphi T}&\boldsymbol{C}_{\varphi\varphi}\end{pmatrix}\begin{pmatrix}\dot{\boldsymbol{d}}_u\\ \dot{\boldsymbol{d}}_T\\ \dot{\boldsymbol{d}}_\varphi\end{pmatrix}+\begin{pmatrix}\boldsymbol{K}_{uu}&\boldsymbol{K}_{uT}&\boldsymbol{K}_{u\varphi}\\ \boldsymbol{K}_{Tu}&\boldsymbol{K}_{TT}&\boldsymbol{K}_{T\varphi}\\ \boldsymbol{K}_{\varphi u}&\boldsymbol{K}_{\varphi T}&\boldsymbol{K}_{\varphi\varphi}\end{pmatrix}\begin{pmatrix}\boldsymbol{d}_u\\ \boldsymbol{d}_T\\ \boldsymbol{d}_\varphi\end{pmatrix}\\ &=\begin{pmatrix}\boldsymbol{f}_u\\ \boldsymbol{f}_T\\ \boldsymbol{f}_\varphi\end{pmatrix}=\begin{pmatrix}\boldsymbol{f}_{uu}+\boldsymbol{f}_{uT}+\boldsymbol{f}_{u\varphi}\\ \boldsymbol{f}_{Tu}+\boldsymbol{f}_{TT}+\boldsymbol{f}_{T\varphi}\\ \boldsymbol{f}_{\varphi u}+\boldsymbol{f}_{\varphi T}+\boldsymbol{f}_{\varphi\varphi}\end{pmatrix},\end{aligned} \tag{4.1}$$

where the subscript u denotes the displacements, the subscript φ denotes the relative humidity and the subscript T denotes the temperature. The vectors $\boldsymbol{d}_u$, $\boldsymbol{d}_T$ and $\boldsymbol{d}_\varphi$ denote

unknown nodal variables, the vectors $\boldsymbol{f}_u$, $\boldsymbol{f}_T$ and $\boldsymbol{f}_\varphi$ denote prescribed nodal forces and fluxes (usually denoted $\boldsymbol{g}$ and $\boldsymbol{q}$ in transport processes, see Eq. (3.29)), the matrices $\boldsymbol{K}$ with subscripts denote the stiffness, conductivity and coupling matrices and the matrices $\boldsymbol{C}$ with subscripts denote the capacity and coupling matrices. The vectors $\boldsymbol{f}_u$, $\boldsymbol{f}_T$ and $\boldsymbol{f}_\varphi$ are further split to three contributions. The vector $\boldsymbol{f}_u$ is the sum of vectors $\boldsymbol{f}_{uu}$, $\boldsymbol{f}_{uT}$ and $\boldsymbol{f}_{u\varphi}$ which represent contributions to the nodal forces from mechanical analysis, temperature changes and humidity changes. The meaning of other contributions is similar.

The system of differential equations (4.1) can be written more compactly in the form

$$\boldsymbol{C}(\boldsymbol{d})\dot{\boldsymbol{d}}+\boldsymbol{K}(\boldsymbol{d})\boldsymbol{d}=\boldsymbol{f}, \tag{4.2}$$

where the dependency of the stiffness, conductivity, capacity and coupling matrices on the attained values of variables is explicitly denoted. $\boldsymbol{d}$ and $\dot{\boldsymbol{d}}$ denote increments of nodal variables and their time derivatives.

The system (4.2) has to be solved by an incremental method. Time discretization is based on the v-form of the generalized trapezoidal method [12] defined by the relationships

$$\boldsymbol{d}_{n+1}=\boldsymbol{d}_n+\Delta t\boldsymbol{v}_{n+\gamma}, \tag{4.3}$$

$$\boldsymbol{v}_{n+\gamma}=(1-\gamma)\boldsymbol{v}_n+\gamma\boldsymbol{v}_{n+1}, \tag{4.4}$$

where $\boldsymbol{v}$ denotes the first derivatives of nodal values with respect to time and γ is a parameter from the range $[0,1]$. The subscript n denotes the time step and it serves also as an index in the incremental method, called the outer iteration loop. It is assumed that all variables are known at the time t_n and variables at the time t_{n+1} are searched.

Substitution of expressions defined in Eqs. (4.3) and (4.4) to the system of differential equations (4.2) leads to relationship

$$(\boldsymbol{C}_n+\Delta t\gamma\boldsymbol{K}_n)\boldsymbol{v}_{n+1}=\boldsymbol{f}_{n+1}-\boldsymbol{K}_n(\boldsymbol{d}_n+\Delta t(1-\gamma)\boldsymbol{v}_n), \tag{4.5}$$

where $\boldsymbol{C}_n$ and $\boldsymbol{K}_n$ denote the capacity and stiffness/conductivity matrices evaluated with the help of values $\boldsymbol{d}_n$. The system of algebraic equations (4.5) is generally non-linear and the Newton-Raphson method [7,8] has to be used at each time step.

The trial solution $\boldsymbol{v}_{n+1,0}$ of the system of equations (4.5) is used for computation of the trial nodal values $\boldsymbol{d}_{n+1,0}$ which are obtained from Eqs. (4.4) and (4.3). Substitution of the trial solution back to the system of equations (4.5) with modified matrices does not generally lead to equality. An iteration loop, called the inner iteration loop, in every time step is based on residual which is computed from the relationship

$$\boldsymbol{r}_{n+1,j}=\boldsymbol{f}_{n+1}-\boldsymbol{K}_n(\boldsymbol{d}_n+\Delta t(1-\gamma)\boldsymbol{v}_n)-\left(\boldsymbol{C}_{n+1,j}+\Delta t\gamma\boldsymbol{K}_{n+1,j}\right)\boldsymbol{v}_{n+1,j}, \tag{4.6}$$

where $\boldsymbol{C}_{n+1,j}$ and $\boldsymbol{K}_{n+1,j}$ denote the matrices evaluated for $\boldsymbol{d}_{n+1,j}$ and j is the index in the inner loop. Correction of nodal time derivatives are computed from the equation

$$\left(\boldsymbol{C}_{n+1,j}+\Delta t\gamma\boldsymbol{K}_{n+1,j}\right)\Delta\boldsymbol{v}_{n+1,j+1}=\boldsymbol{r}_{n+1,j} \tag{4.7}$$

and new time derivatives are in the form

$$\boldsymbol{v}_{n+1,j+1} = \boldsymbol{v}_{n+1,j} + \Delta \boldsymbol{v}_{n+1,j+1}\,. \tag{4.8}$$

It has to be noted that the permanent recalculation of matrices $\boldsymbol{K}$ and $\boldsymbol{C}$ with respect to actual nodal values is very computationally demanding. In such a case, the matrix of the system of equations $\boldsymbol{C}(\boldsymbol{d}) + \Delta t \gamma \boldsymbol{K}(\boldsymbol{d})$ has to be always factorized and it requires additional computational time. The numerical examples show that the modified Newton method, which changes the system matrix only at the beginning of a new time step is the best choice.

5 Implementation

Implementation of numerical methods, material models and tools for parallel computing has to satisfy several contradicting requirements. Easy extensibility of a code is probably the most important requirement. Another important requirement is connected with code performance. These two basic requirements on a code are definitely contradictory because really very efficient implementation of a numerical method differs significantly from description of the method in textbooks and therefore the orientation in the code is much more difficult.

The computer code SIFEL developed at our department is written in the C++ language and can be found at the web address [32]. The attention is not concentrated on particular programming language but rather on suitable formulation of the problem and correct analysis. Detailed analysis of a system of non-linear ordinary differential equations (4.1) reveals similarity of particular submatrices. The stiffness and conductivity matrices (denoted by $\boldsymbol{K}$ with appropriate subscripts) have generally the form

$$\boldsymbol{K}_{ij} = \int_{\Omega} \boldsymbol{B}_i^T \boldsymbol{D}_{ij} \boldsymbol{B}_j \mathrm{d}\Omega, \tag{5.1}$$

where $\boldsymbol{B}_i$ and $\boldsymbol{B}_j$ denote the gradient matrices, $\boldsymbol{D}_{ij}$ denotes the matrix of stiffness or conductivity of the material and the subscripts i and j substitute any of subscripts u, T or φ. Similarly, the capacity matrices (denoted by $\boldsymbol{C}$ with appropriate subscripts) have generally the form

$$\boldsymbol{C}_{ij} = \int_{\Omega} \boldsymbol{N}_i^T \boldsymbol{H}_{ij} \boldsymbol{N}_j \mathrm{d}\Omega, \tag{5.2}$$

where $\boldsymbol{N}_i$ and $\boldsymbol{N}_j$ denote the matrices of base functions and $\boldsymbol{H}_{ij}$ denotes the matrix of material parameters.

For better understanding, the following extension of the mechanical analysis is presented. Let an elastic material be assumed. The constitutive equation (Hook's law) has the form

$$\boldsymbol{\sigma} = \boldsymbol{D}_{uu} \boldsymbol{\varepsilon}(\boldsymbol{u}) \tag{5.3}$$

and it relates the strains $\boldsymbol{\varepsilon}(\boldsymbol{u})$ and stresses $\boldsymbol{\sigma}$. $\boldsymbol{D}_{uu}$ is the stiffness matrix of the material. It should be noted that the strains depend on displacements $\boldsymbol{u}$ which are discretized and the nodal displacements are denoted by $\boldsymbol{d}_u$. The mechanical problem with negligible inertial forces can be written in the form

$$\boldsymbol{K}_{uu}\boldsymbol{d}_u = \boldsymbol{f}_u, \tag{5.4}$$

where $\boldsymbol{K}_{uu}$ denotes the stiffness matrix of structure and $\boldsymbol{f}_u$ denotes the vector of prescribed nodal forces. Eq. (5.4) expresses the equilibrium condition.

If the temperature plays a role, the constitutive relationship (5.3) has to be replaced by the following constitutive equation

$$\boldsymbol{\sigma} = \boldsymbol{D}_{uu}\boldsymbol{\varepsilon}(\boldsymbol{u}) + \boldsymbol{D}_{uT}\nabla T, \tag{5.5}$$

where T is the temperature and $\boldsymbol{D}_{uT}$ denotes the matrix of material coefficients. Moreover, the constitutive relationship between the heat flux $\boldsymbol{q}$ and the temperature gradient is needed and it has the form

$$\boldsymbol{q} = \boldsymbol{D}_{TT}\nabla T, \tag{5.6}$$

where $\boldsymbol{D}_{TT}$ is the conductivity matrix of material. It is usually accepted that the heat flux is independent of the displacements $\boldsymbol{u}$. The equilibrium condition (5.4) is therefore extended with the heat balance equation and the system of equations has the form

$$\begin{pmatrix} \boldsymbol{K}_{uu} & \boldsymbol{K}_{uT} \\ \boldsymbol{0} & \boldsymbol{K}_{TT} \end{pmatrix} \begin{pmatrix} \boldsymbol{d}_u \\ \boldsymbol{d}_T \end{pmatrix} = \begin{pmatrix} \boldsymbol{f}_u \\ \boldsymbol{f}_T \end{pmatrix}, \tag{5.7}$$

where $\boldsymbol{d}_T$ is the vector of nodal temperatures and $\boldsymbol{f}_T$ is the vector of prescribed nodal heat fluxes. The first equation in the system (5.7) expresses the equilibrium condition while the second equation in the system (5.7) expresses the heat balance condition. The zero block in the heat balance equation determines the independence of the heat transfer on the mechanical problem but on the contrary, the mechanical problem is coupled with the heat transfer.

Additional variables can be introduced in the constitutive equations and additional balance equations can be added to the system. The thermo-mechanical problem (5.7) extended by the relative humidity and capacity terms result in the form (4.1).

The previous analysis of the structure of system (4.1) offers directly the instruction for efficient implementation. Our implementation of the coupled hydro-thermo-mechanical problems is based on three independent modules. The first module, MEFEL, is an independent computer code for mechanical analysis which can stand alone. It means, the code is able to deal with the pure mechanical analysis. It assembles submatrix $\boldsymbol{K}_{uu}$ and subvector $\boldsymbol{f}_{uu}$ from system (4.1). The second module, TRFEL, is an independent computer code for heat and moisture transfer which can also be used separately. It assembles the submatrices $\boldsymbol{K}_{TT}$, $\boldsymbol{K}_{T\varphi}$, $\boldsymbol{K}_{\varphi T}$, $\boldsymbol{K}_{\varphi\varphi}$, $\boldsymbol{C}_{TT}$, $\boldsymbol{C}_{T\varphi}$, $\boldsymbol{C}_{\varphi T}$, $\boldsymbol{C}_{\varphi\varphi}$ and subvectors $\boldsymbol{f}_{TT}$, $\boldsymbol{f}_{T\varphi}$, $\boldsymbol{f}_{\varphi T}$,

$f_{\varphi\varphi}$. The coupling between the mechanical and transport part is implemented in the third module, METR, which deals with the off-diagonal terms in the coupled problem. It means, this module assembles the submatrices $\boldsymbol{K}_{uT}$, $\boldsymbol{K}_{u\varphi}$, $\boldsymbol{K}_{Tu}$, $\boldsymbol{K}_{\varphi u}$, $\boldsymbol{C}_{uT}$, $\boldsymbol{C}_{u\varphi}$, $\boldsymbol{C}_{Tu}$, $\boldsymbol{C}_{\varphi u}$ and the subvectors f_{uT}, $f_{u\varphi}$, f_{Tu} and $f_{\varphi u}$.

At this time, many concepts of merging software especially based on Python language can be found in literature. These concepts combine the existing computer codes and the exchange data among them. Unfortunately, a fully coupled analysis cannot be attained by these concepts. They result in staggered algorithms. In our concept, we do not merge the whole codes but we are using suitable subroutines from particular codes. The coupled problems are solved by the third module, METR, which uses many subroutines from the MEFEL and TRFEL codes. Of course, new subroutines dealing with the coupling terms had to be implemented. For better understanding, the numbers of lines of the source code are summarized. The MEFEL code contains approximately 210,000 lines, the TRFEL code contains 120,000 lines and the METR code contains 30,000 lines. It is clear that the number of lines of source code in METR is larger than is the usual number of lines in the Python merging code. On the other hand, it enables staggered as well as fully coupled analysis and the resulting code is compiled and therefore very fast.

Additional advantage stems from the fact that any improvement of the mechanical or transport module is automatically projected to the code for coupled problems. It is also very convenient for developers which can deal with one part of the whole code.

Modelling of the sequential construction of a structure is another important requirement on the software for civil engineering problems. There are many possibilities for implementation of this feature. Some programs use a transfer of results from the mesh of the calculated stage to the next one via files but SIFEL uses more efficient implementation. The mesh is generated for all construction stages at once and individual parts of the mesh are switched on and off by the state time functions specified for each element. Changes in the state of elements are monitored in the course of time and if there is a change, the nodal degrees of freedom are renumbered automatically.

The program can solve stationary and non-stationary, linear and non-linear problems of heat and moisture transfer as well as linear and non-linear statics, eigenvibrations, dynamics and time dependent problems with negligible inertial forces. A 2D and 3D domain can be modeled by various types of finite elements. The SIFEL has implemented the bar, triangular, quadrilateral, tetrahedron and hexahedron elements where both types of approximation functions, linear and quadratic, can be used.

5.1 Material models

The matrices defined by (5.1) and (5.2) are assembled with respect to the used material models. The proper selection of a material model is the key point in the analyses of real engineering and scientific problems. The implementation of material models consists in writing several functions connected with the evaluation of the material matrices and stresses or fluxes. There is no need for rewriting the other module parts such as

the routines dealing with elements. It can be demonstrated on the implementation of a new mechanical material model. In such a case, the user have to write the following procedures containing:

- reading of material parameters,
- assembling of the material stiffness matrix,
- computation of the stresses from the given strains,
- update of internal variables of the material model.

Both the modules TRFEL and MEFEL contain a number of material models. Many of them describe behaviour of concrete or soils because our team is focused on civil engineering problems where these materials play an important role.

The models implemented in MEFEL can be split into several main categories such as plasticity (J2 flow, Drucker-Prager, Mohr-Coulomb, Cam-Clay, HISS and Chen models), damage (scalar isotropic, orthotropic and anisotropic damage models), creep (Bazant's B3, simple viscoplasticity) and other (Microplane M4).

In the TRFEL module, there are implemented several material models, approaches and theories for heat transfer, moisture transfer, coupled heat and moisture transport, coupled heat-moisture and salt transport with phenomenological based models (Künzel and Kiessl, Grunewald, Pedersen) and micromechanical based models (Lewis and Schrefler, Tenchev). Various types of sorption isotherms and moisture storage functions are also implemented (Root, Hansen, Bazant, Baroghel-Bouny), functions for experimentally measured data and non-linear behaviour of material parameters (heat conductivity, capacity, permeability, etc.) The code allows to describe different types of boundary and initial conditions, e.g. Dirichlet boundary conditions (prescribed temperature, moisture, relative humidity, etc.), Neumann b. c. (prescribed fluxes of heat and mass), Cauchy b. c. (heat transfer on boundary, diffusion effect), climatic conditions exposure (wind effect, rain, water contact, heat transfer and moisture diffusion, short and long wave radiation) and the heat source condition, e.g. measured data from calorimetry, multiscale modelling of cement hydration process based on the model CEMHYD3D [35], etc.

6 Solved problems

Development of the SIFEL package was motivated by real civil engineering problems that were solved at our department. The software was used for a variety of problems starting with dynamics of bridges, rock slope stability, analysis of tunnel sheeting, foundation slabs and finishing with complex coupled problems such as analysis of a nuclear power plant containment.

A complex analysis of the reactor vessel in the UK was the first coupled problem solved with METR. The problem was solved within the scope of European project MAECENAS whose topics were connected with prolongation of the service life of nuclear power plants. The problem was solved as a coupled thermo-hydro-mechanical analysis

and more details can be found in [22].

The problem of the lift layer separation on bridge decks was another coupled thermo-hydro-mechanical analysis solved using METR. This problem was observed during reconstruction of bypass road bridge in Valašské Meziříčí (Czech Republic). The reconstructed lift layer was relatively thin (10∼12 cm) and it caused large crack propagation due to shrinkage. In addition, the important role of climate conditions during casting was acknowledged. Proper curing procedure and reinforcement were proposed on the basis of the performed analyses which are described in paper [16].

The most complex coupled problems solved by METR are presented in the following subsections. High demands of these problems were caused by complex geometry, the amount of modelled details, complexity of material models and the high number of performed time steps.

6.1 Watertightness of foundation slabs

High performance concrete in the diaphragm walls and foundation slabs was one of the topics of the CIDEAS project in whose scope, the research of watertightness of foundation slabs was carried out. The motivation of this research was the construction of a commercial building in Prague (Czech Republic) near the Vltava river. The building was founded on a slab 10 meters under the ground-water level which led to the increased demands on watertightness of the used concrete.

Foundation slabs are often built in deep ditches under the ground-water level and they can have a significant thickness. The watertightness is influenced by a variety of factors, especially:

- concrete mixture composition,
- degree and form of reinforcement,
- technology of casting procedure,
- arrangement of working gaps,
- proper curing of concrete during hydration.

Watertight concrete is often designed as high-performance, self-compacting or easy-compacting where, except the basic material parameters such as water-cement ratio and particular aggregates, an important role also play the admixtures such as superplastifiers and accelerators. These admixtures influence significantly evolution of hydration heat and autogeneous shrinkage whose values are raised when compared to the usual concrete.

These factors are necessary to take into account in computer simulation of slab behaviour. The computer simulation should represent

- used casting procedure by particular layers and shrinkage parts (the slab has to be cast in several layers with thickness 400∼600 mm),
- curing of concrete (watering and protection against sun radiation),

- autogeneous shrinkage in early stages,
- drying shrinkage in late stages,
- increasing stiffness and strength of concrete in course of time,
- creep of concrete,
- possible damage of concrete.

All these effects depend on time, temperature and humidity and thus the coupled thermo-hydro-mechanical analysis should be performed.

The foundation slab of the mentioned commercial building in Prague was analyzed by a staggered approach where the transport processes influenced the mechanical analysis. It should be emphasized that the heat and moisture transfer were fully coupled.

The slab is created from two parts which are mutually shifted 1.3 m. The thickness of slab is 1 m and the spans are 15.0 and 15.8 m. On the boundaries are left shrinkage bands whose width is 1.5 m. The scheme of the slab is depicted in Fig. 1.

The slab was reinforced by 12 bars of reinforcement V25 per meter in longitudinal and transversal directions. There were also ties made from reinforcement V16 whose density was 9 pieces per square meter.

The slab was cast in three layers of the thickness of approximately 33 cm in order to avoid the damage due to the generated hydration heat. The cast sections were watered for three days and they were covered by PE sheets after casting. The generation of hydration heat during first several hours and damage evolution due to shrinkage and thermal strains were the reasons for small time steps used at the beginning of analysis. Damage evolution causes the increase of the norm of the unbalanced force vector in the Newton-Raphson method and if the time step is not chosen carefully, convergence problems arise.

The computer simulation begins at 1 hour after the end of casting of the first layer. In the performed thermo-hydro-mechanical analysis, the Künzel-Kiessl's model was used for modelling of transport processes, the B3 creep model and the scalar isotropic damage model were used for the description of the mechanical behaviour. These models were in SIFEL computer code complemented by a hydration heat model for concrete and by statistically processed data of climatic conditions for Prague region. The slab was supported by springs at the bottom. Stiffness of the springs near the corners were increased in order to capture of subsoil behaviour. A dead weight load was applied on the whole slab. An important role was played by the thermal boundary conditions used in the heat transfer analysis. In this case, thermal boundary conditions simulated the average aerial daily temperatures in June and they were obtained by long-term measurements in the given region.

Thermo-hydro-mechanical coupled problems have very large demands on computational power. Because many material models were coupled together, an extraordinarily large number of internal variables were stored in each integration points. The stored internal variables and the large matrix of the system of algebraic equations led to extremely large demands on computer memory. In this case, the memory space used for internal variables and memory space used for the system matrix are comparable. Taking

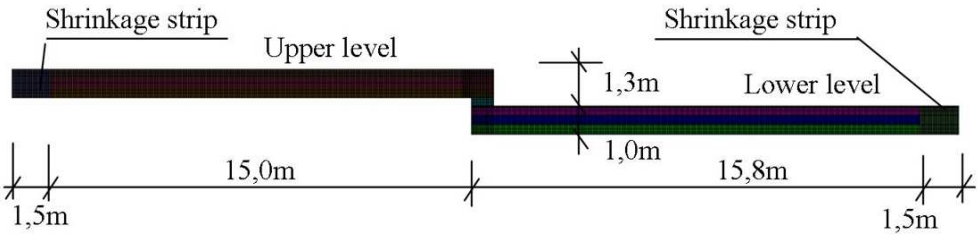

Figure 1: Dimensions of the model and finite element mesh – section view.

into account the memory requirements, the 2D model of the problem was created even though the program can solve 3D problems as well as the material models are derived for 3D too. The use of 2D elements reduces the number of both internal variables and unknowns. The reduced number of unknowns is also important for the speed of factorization of the equation system (4.5). The factorization has to be performed once or several times at each time step depending on the results from the Newton-Raphson method that has to be used due to non-linearities hidden in the scalar isotropic damage model.

The sizes of finite elements used were about 4 cm in both directions except of the thin bottom and top layers where the mesh is twice finer in the transversal direction. The necessity of the finer mesh is given by increased temperature and humidity gradients in these layers and the consequent damage occurrence. Details of mesh decomposition are captured in Fig. 2.

The generated mesh takes into account the sequential casting procedure and the particular concrete layers are generated with different material properties. In Figs. 1 and 2, these layers are drawn by various colours.

B3 model was used for the creep and shrinkage description, which involves evolution of Young's modulus with respect to age of concrete while the scalar isotropic damage model assumed the material parameters to be constant. It was especially necessary to introduce a time dependent evolution of the tensile strength. In this case, a simple linear function was assumed

$$f_t(t) = cE(t), \tag{6.1}$$

where c is material parameter and $E(t)$ is the value of time dependent Young's modulus which was calculated by the B3 model. The material parameters for concrete class C35/45 were used in the B3 model and c was set to 10^{-4}.

Two conclusions follow from the results of the coupled heat and moisture transfer analysis and from the simultaneous mechanical analysis. The first is that the accumulated hydration heat expires approximately after 7 days (Fig. 3) simultaneously with autogeneous shrinkage phase. The second conclusion is that during the process of drying, the drop of moisture content and temperature occurs first in the surface layers and much later in the core. The effect of the diffusion process of drying (shrinkage of concrete) on the stress development and micro-cracks distribution is rather extensive. Smeared cracks can cause the initialization of main cracks.

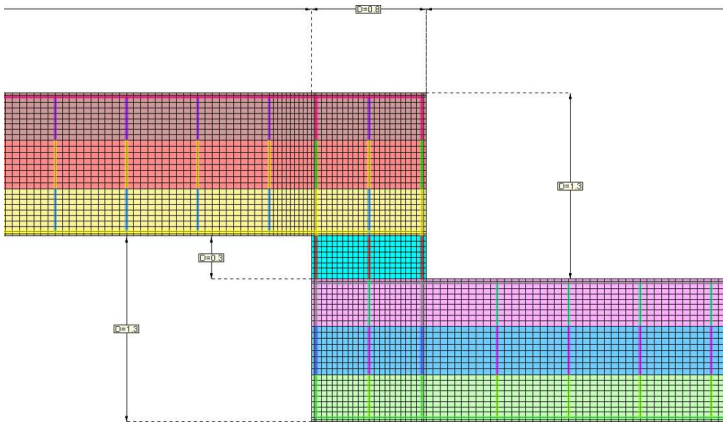

Figure 2: Detail of FE mesh near drop.

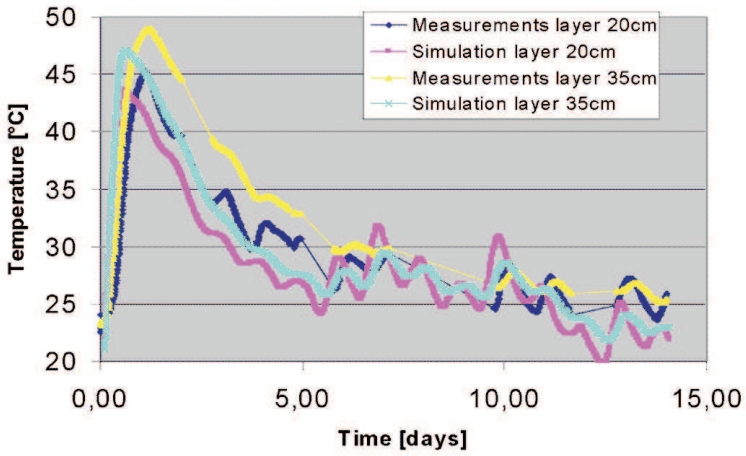

Figure 3: Temperature history.

The following figures depict the resulting course of the normal stresses σ_x (Fig. 4), the shear stresses τ_{xy} (Fig. 5), the deformed shape of the structure (Figs. 6-8) and the damage parameter ω (Figs. 9-11) for particular construction stages of the lower slab. The results were calculated at the time shortly before the casting of the next layer for the two bottom layers and for the top layer, they were calculated at the time of 15 hours since casting of the first layer. Detailed views of the damaged areas are captured in Figs. 12 and 13.

The results of the analysis confirmed that the correct modelling of the sequential construction influences the evolution of the damage parameter significantly. In Fig. 12, the distribution of nonzero values of the damage parameter can be seen on the bottom layer which extends to 20 cm of its thickness. The maximum value of the damage parameter is 0.4. The damage is caused by hydration heat generation of the top layer which is delayed when compared to the bottom layers. The peak of hydration heat generation in the top

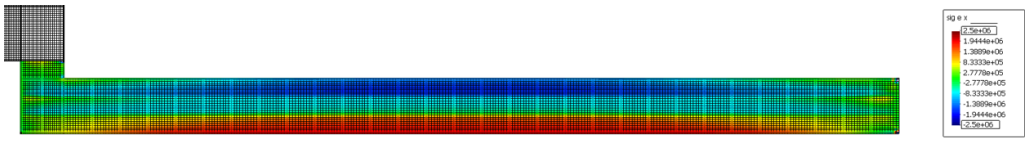

Figure 4: Distribution of stresses σ_x.

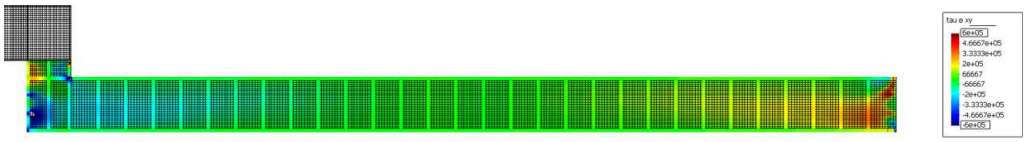

Figure 5: Distribution of stresses τ_{xy}.

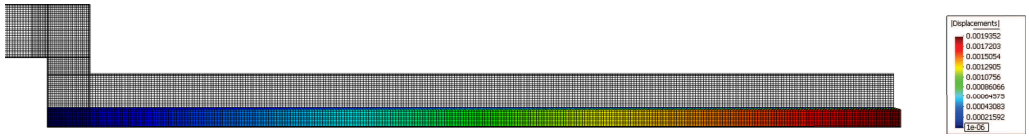

Figure 6: Deformed shape of the first layer of concrete.

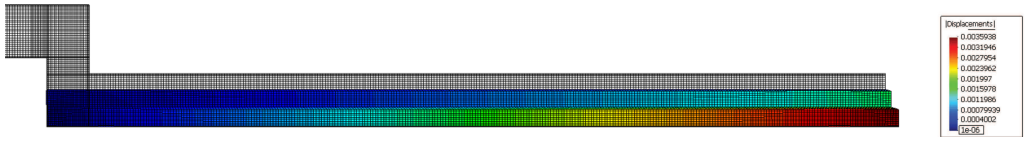

Figure 7: Deformed shape of the second layer of concrete.

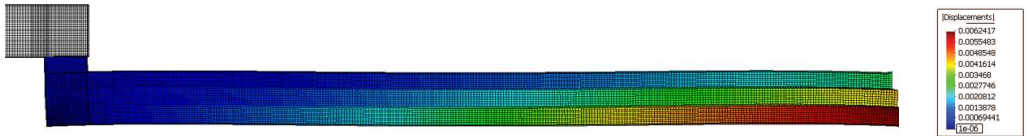

Figure 8: Deformed shape of the third layer of concrete.

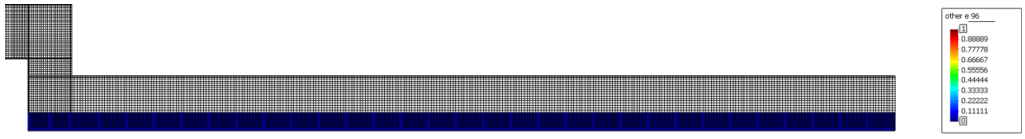

Figure 9: Distribution of the damage parameter ω in the first layer of concrete.

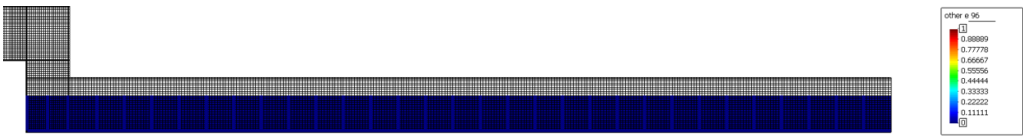

Figure 10: Distribution of the damage parameter ω in the second layer of concrete.

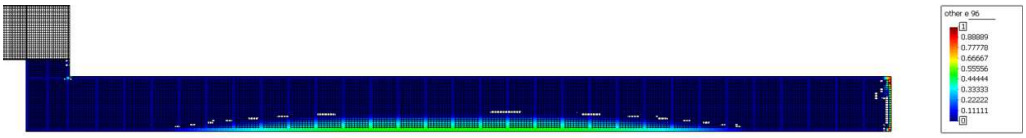

Figure 11: Distribution of the damage parameter ω in the third layer of concrete.

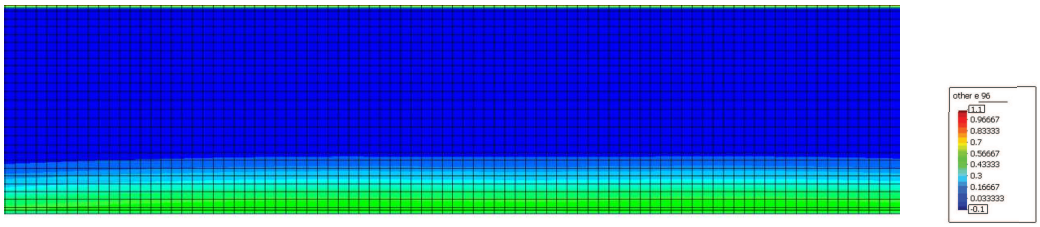

Figure 12: Distribution of the damage parameter ω in the middle of the slab.

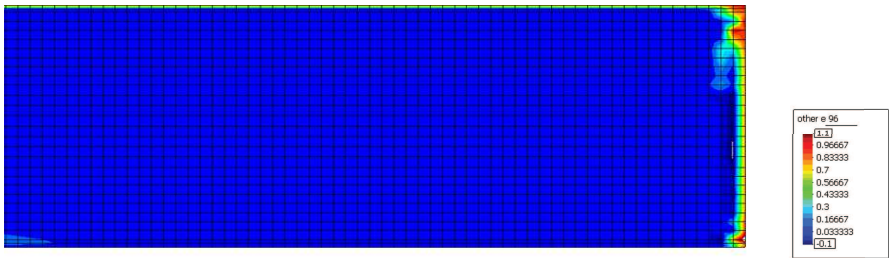

Figure 13: Distribution of the damage parameter ω in the right corner of the slab.

layer causes nonuniform distribution of thermal strains and consequently, the slab tends to deflect upward. In the middle of the slab, the influence of dead weight load dominates and it leads to the damage of the bottom layer. The resulting deformed shape of the structure is captured in Fig. 8.

Another factor causing damage are the climate conditions. It can be observed in Fig. 12 that the whole top surface is damaged but only to a shallow depth. The damage was caused by drying shrinkage which was intensified by the applied climatic conditions. The last area with significant damage evolution is at the top right corner of the slab (see Fig. 13). In this case, the damage was caused by shear stresses whose concentration at the corner can be observed in Fig. 5.

6.2 Computer simulation of reactor vessel

Reliability and durability of reactor containments depend directly on the prestressing system. General results from in-situ measurements during the whole time of operation show the increase of deformations and the increase of prestress losses since the onset of service. Most measurements also indicate that the temperature has a major influence on the prestress losses. These conclusions were obtained, e.g., from thirty years of measured prestress at Swedish nuclear reactor containments [1]. This section presents a computer simulation of a nuclear power plant containment under cyclic temperature loading during service, when stages of service and planned stops are changed. It is well known that the increase of temperature influences the rate of concrete creep. This fact can cause significant prestress losses of the structure. Moreover, increasing deformations are observed and additional cracks could occur. An advanced two-level model is used for predicting the prestress losses and the structure response. It is a combination of a global macro-level model and a local model. The aim of the global one is the modelling of evolution of prestress forces changed by the temperature and climatic loading. The local model is loaded by the mechanical and thermal loading from the global model. The staggered coupled thermo-mechanical analysis is the main part of the local model which has to explain the time dependent processes in the containment wall. The heat transfer analysis is running in parallel with the mechanical analysis where the temperature effect on concrete creep is modeled by Bazant's microprestress-solidification theory. The local model is subsequently completed by suitable damage models.

The presented study is a part of the global reliability and durability model of nuclear power plant containment in Temelín in the Czech Republic. The presented computation attempts to model and explain the increase of radial deformation and decreasing of tendon forces since the onset of service. There was a lot of measurements to explain this phenomena at Swedish nuclear reactor containment with non-injected (non-bounded) prestress tendons [1] in the time period of 5 years (6.5 years in Czech Republic). Time evolution of the tendon force is plotted in logarithmic scale in Fig. 14.

Two gradients of the tendon force losses were also observed in prestress measurements at the Czech containment. With reference to [1] and discussions in theoretical studies [5] and [11], it can be concluded that the increase of temperature influences acceleration of creep. Every change of temperature, moisture content, and loading causes changes of creep rate [5]. There is no doubt that the temperature is one of the sources of prestress losses increase. The influence of temperature will be the dominant phenomenon, the damage will have the minor effect, and the radial strains increase will be neglected.

6.2.1 Basic data

The containment of the nuclear power plant in the Czech Republic is a monolithic post-tensioned structure made from reinforced concrete. It consists of two parts – the lower cylindrical part and the upper dome. The cylinder has the internal diameter of 45.00 m

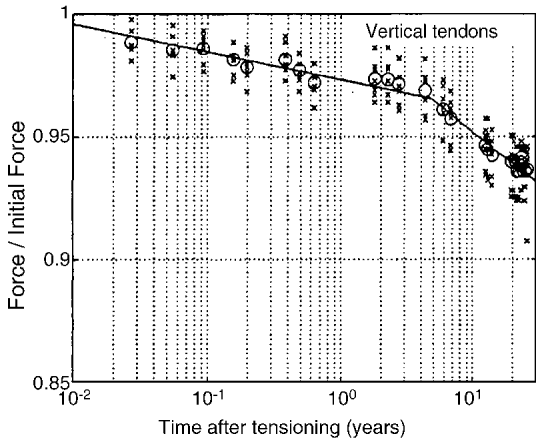

Figure 14: Change of tendon force gradient since service time [1].

and the wall is 1.20 m thick. The dome is fixed into a massive girder. The scheme of the structure is in Fig. 15. The leak-proofness of the containment is secured by the 8 mm thick steel lining placed inside the structure. Unbonded tendons are placed in three parallel layers in the containment wall.

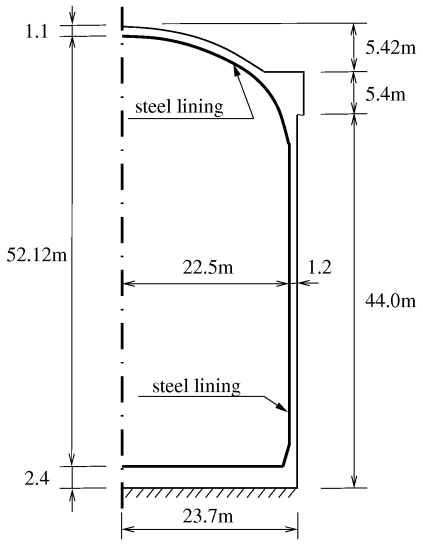

Figure 15: Geometry – section view of the containment.

6.2.2 Local model

Geometry. The local model – the cylindrical segment represents a periodic unit cell (PUC) from the cylindrical part of the containment with channels for prestressing tendons and with vertical, radial and horizontal reinforcement. It is captured in Fig. 17.

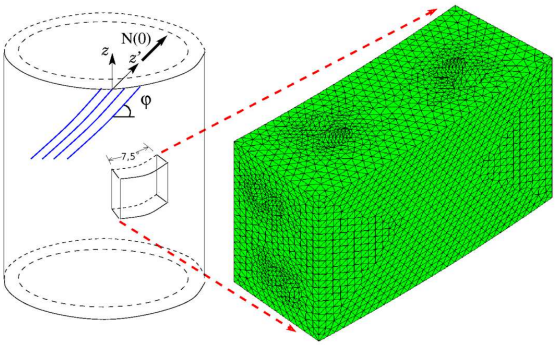

Figure 16: Scheme of PUC.

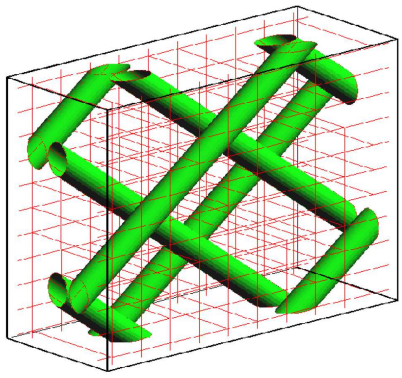

Figure 17: Tendon channels and reinforcement.

The height of PUC is 2.12 m and it covers the section of the angle of 7.5° (Fig. 16). The prestressing tendons are not modeled. Their effect is introduced as mechanical loading.

The finite element mesh was generated by the automatic mesh generator T3D [39]. The thermo-mechanical coupled algorithm of the finite element computer code SIFEL [32] was used.

6.2.3 Loading

Temperature loading. The impact of temperature is modeled by the Dirichlet boundary conditions. Temperatures from in-situ measurements (inner and outer surface) are applied directly into computation. The temperature cycle loading depicted in Fig. 18 was considered in one year intervals.

Mechanical loading. Mechanical loading of the cylindrical segment is considered as a combination of four types of loading: (i) Dead weight of the segment. (ii) Dead weight

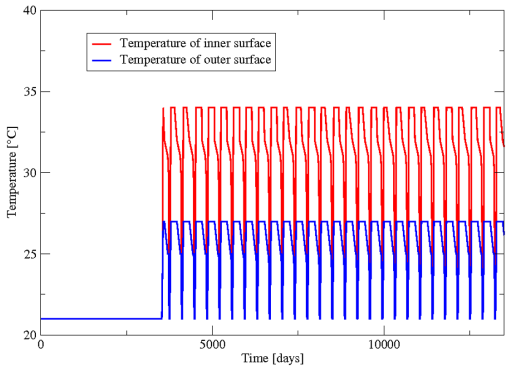

Figure 18: Temperatures of inner and outer surface considered in the computer simulation since the end of construction.

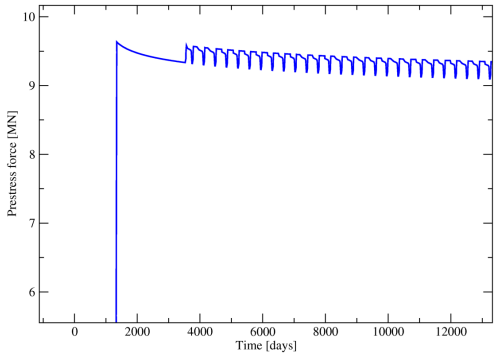

Figure 19: Change of the prestress force in the anchorage system since the end of construction.

of the containment over the segment is considered as a loading on the top surface. (iii) Vertical loading of the prestress forces is considered also as loading on the top surface. It is computed from the reactions of the anchorage system decreased by prestress losses caused by friction in tendon channels. (iv) Loading prescribed directly in tendon channels is consisting of radial and tangential components.

The first two loadings are instantaneous. The latter two loadings are calculated as a multiple of prestress forces in tendons in place of the anchorage system. The values of prestress forces are obtained from in-situ measurements by a magneto-elastic method (MEM) and they are displayed in Fig. 19. The data were approximated by a logarithmic regression method. In the graph, jumps which simulate in the cycle service time – the planned stop are obtained from the global model.

Material properties and equations. In the transport part of the problem, the non-stationary heat transport was solved assuming constant material parameters. The mechanical part of the computation considered four types of constitutive material models, namely creep, damage, plasticity and the thermal dilatation. The B3 creep model influenced by temperature and moisture changes and a damage model describe the behaviour of concrete. Several damage models were used in the computer simulation. There were local and non-local versions of scalar isotropic damage model, anisotropic damage model and orthotropic model. Results obtained using the orthotropic model showed the best coincidence with in-situ measurements. The application of damage models is described in detail in [17]. The steel reinforcement was modeled using the bar finite elements with plasticity model using Huber-Mises-Hencky condition. The thermal dilatation model was assumed in both materials (concrete and reinforcement).

6.2.4 Results of computation and conclusions

The relation between the response of the local model and the tensile strength of concrete in damage models was observed during the computer simulation. Hence, there were made several calculations with different tensile strengths in order to verify the damage evolution. The scalar isotropic damage model gives the upper estimate because the damage parameter influenced all principal directions.

Therefore, the more realistic anisotropic or orthotropic models should be used in a reliable prognosis of the containment durability. The distribution of damage parameter for orthotropic damage model is captured in Fig. 20.

From the concrete creep point of view, the different levels of the temperature effect on concrete creep were also studied. In term of explanation of the increase of radial deformation, the most monitored graphs are strains in radial reinforcement depicted in Fig. 21. It can be concluded from the data of the analysis that the temperature effect, which increases concrete creep, is vanishing in time. In the case of some accompanying effect due to cracking strain evolution, the increase of radial deformation and decreasing of tendon forces during service life can be observed. The strains in the radial reinforcement are plotted in Fig. 21 in comparison with the average data from in-situ measurements.

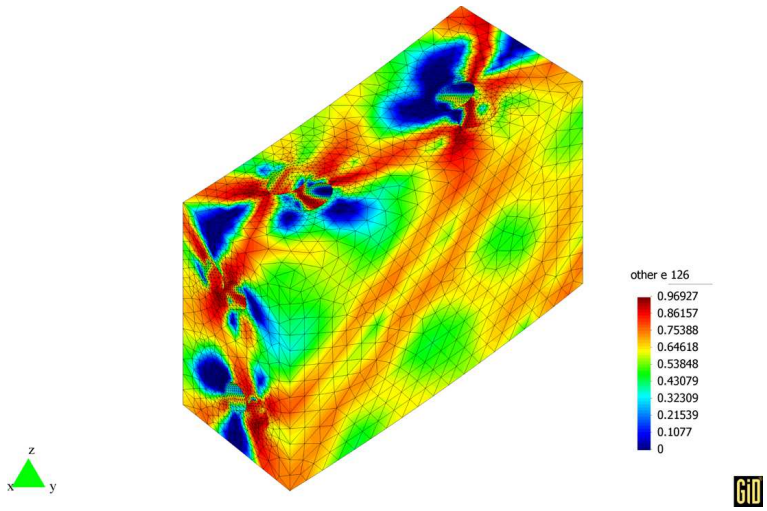

Figure 20: Isosurfaces of damage parameter in time of 6000 hours since the end of construction.

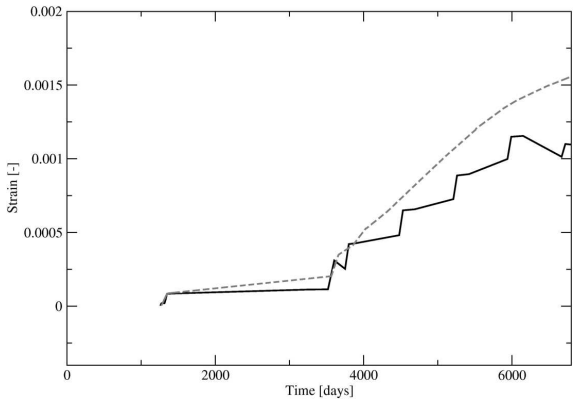

Figure 21: Comparison of strain in radial reinforcement obtained from computation (solid line) and from in-situ measurements (dashed line – averaged data).

Conclusions from the results of analysis are the following:

- The explanation of the increase of radial strains and decreasing of tendon forces since the onset of service is based on the theoretical knowledge in concrete creep influenced by the temperature changes and partly on the prestress losses measurements mainly at Swedish nuclear reactor containments. The influence of the temperature increase during the service was proved.
- The results obtained from the connection of the simplified global model and the local model show relatively good coincidence with in-situ measurements.
- For the best coincidence between the computer simulation and the measurements, calibration of all appearing material models and their parameters should be per-

formed and compared with laboratory and in-situ measurements. Especially, the tensile strength which is the basic property for monitoring the hypothetical damage of the containment has to be determined.

7 Conclusions

The coupled hydro-thermo-mechanical analysis was successfully used for description of behaviour of several complicated concrete structures. Creep and damage models were coupled with heat and moisture effects which enabled description of structure response from construction till the end of service life. In several cases, parallel computers were used because of the extremely large demands on computer memory and power. Future development will be devoted to multiscale modelling which can lead to better results, especially in the early stages of concrete. The application of hp-version of the finite element adaptivity is promising because it reduces the number of unknowns and therefore the computer memory.

Acknowledgments

Financial support for this work was provided by the Czech Science Foundation, projects n. 103/08/1119 and 105/10/1682. Another financial support was provided by the Ministry of Education, Youth and Sports of the Czech Republic, project No. 1M0579. The financial support is gratefully acknowledged.

References

[1] P. Anderson, Thirty years of measured prestress of Swedish nuclear reactor containment, Nucl. Eng. Des, 235 (2005), 2323-2336.
[2] Z. P. Bazant, Mathematical Modeling of Creep and Shrinkage of Concrete, John Wiley&Sons, Chichester-Singapore, 1988.
[3] Z. P. Bazant and S. Baweja, Creep and Shrinkage Prediction Model for Analysis and Design of Concrete Structures – Model B3, Mater. Struc, 28 (1995) 357-365.
[4] Z. P. Bazant and Chern (1985a) Concrete creep at variable humidity: constitutive law and mechanism. Mater. Struc, (RILEM, Paris), 18, Jan., 1-20.
[5] Z. P. Bazant, G. Cusatis and L. Cedolin, Temperature effect on concrete creep modeled by microprestress-solidification theory, J. Eng. Mech-ASCE, Vol. 130, N. 6 (2004), 691-699.
[6] Z. P. Bazant, L. J. Najjar (1972) Nonlinear water diffusion in nonsaturated concrete structural analysis program. Matériaux et constructions, RILEM, Paris, 5(25), 8-9.
[7] Z. Bittnar and J. Šejnoha, Numerical Methods in Structural Mechanics, ASCE Press, New York, USA, 1996.
[8] M. A. Crisfield, Non-linear Finite Element Analysis of Solids and Structures, John Wiley & Sons Ltd, Chichester, UK, 1991.
[9] C. Farhat and F. X. Roux, Implicit parallel processing in structural mechanics, Comput. Mech. Adv., 2 (1994), 1-124.

[10] D. Gawin, C. E. Majorana, B. A. Schrefler (1999) Numerical analysis of hygro-thermic behaviour and damage of concrete at high temperature. Mech. Cohes-Frict. Mat, 4, 37-74.
[11] C. Hellmich, Shotcrete as Part of the New Austrian Tunneling Method: From Thermochemomechanical Material Modeling to Structural Analysis and Safety Assessment of Tunnels, Begutachter: H.A. Mang, F-J Ulm; Institute for Strength of Materials, Vienna University of Technology, Vienna, Austria, 1999.
[12] T. J. R. Hughes, The Finite Element Method. Linear Static and Dynamic Finite Element Analysis, Prentice-Hall, inc. Englewood Cliffs, New Jersey, 1987.
[13] M. Jirásek and Z. P. Bazant, Inelastic Analysis of Structures, John Wiley&Sons, Ltd, Chichester, UK, 2002.
[14] K. Kiessl, Kapillarer und dampfförmiger Feuchtetransrport in mehrschichtigen Bauteilen. PhD Thesis, University of Essen, Essen (1983).
[15] J. Kočí, V. Kočí, J. Maděra, P. Rovnaníková and R. Černý, Computational analysis of hygrothermal performance of renovation renders, Advanced Computational Methods and Experiments in Heat Transfer, XI (2010), 267-277.
[16] T. Koudelka and T. Krejčí, An Anisotropic Damage Model for Concrete in Coupled Problems, Proceedings of the Ninth International Conference on Computational Structures Technology, B. H. V. Topping and M. Papadrakakis, Civil-Comp Press, Stirlingshire, UK, 2008, paper 157.
[17] T. Koudelka, T. Krejčí and J. Šejnoha, Analysis of a Nuclear Power Plant Containment, Proceedings of the Twelfth International Conference on Civil, Structural and Environmental Engineering Computing, B. H. V. Topping, L. F. Costa Neves and R. C. Barros, Civil-Comp Press, Stirlingshire, UK, 2009, paper 132.
[18] T. Krejčí, T. Koudelka, J. Šejnoha and J. Zeman, Computer Simulation of Concrete Structures subject to Cyclic Temperature Loading, Proceedings of the Twelfth International Conference on Civil, Structural and Environmental Engineering Computing, B. H. V. Topping, L. F. Costa Neves and R. C. Barros, Civil-Comp Press, Stirlingshire, UK, 2009, paper 131.
[19] J. Kruis, Domain Decomposition Methods on Parallel Computers, Progress in Engineering Computational Technology, B. H. V. Topping and Mota Soares, C. A., Saxe-Coburg Publications, Stirling, Scotland, UK, (2004), 299-322.
[20] J. Kruis, Domain Decomposition Methods for Distributed Computing, Saxe-Coburg Publications, Kippen, Stirling, Scotland, UK, 2006.
[21] J. Kruis, The FETI Method and its Applications: A Review, Parallel, Distributed and Grid Computing for Engineering, B. H. V. Topping, and P. Iványi, Saxe-Coburg Publications, UK, (2009), 199-216.
[22] J. Kruis, T. Koudelka and T. Krejčí, Efficient computer implementation of coupled hydro-thermo-mechanical analysis, Math. Comput. Simulat, 80 (2010), 1578-1588.
[23] H. M. Künzel and K. Kiessl, Calculation of heat and moisture transfer in exposed building components, Int. J. Heat Mass Tran, 40 (1997), 159-167.
[24] J. Lemaitre and J. L. Chaboche, Mechanics of solid materials, Cambridge University Press, Cambridge, UK, 1994.
[25] J. Maděra, J. Kočí, V. Kočí, J. Výborný and R. Černý, Computational prediction of hygrothermal conditions in innovated AAC-based building envelopes, Advanced Computational Methods and Experiments in Heat Transfer, XI (2010), 291-301.
[26] C. Majorana, J. Mazars, Thermohygrometric and mechanical behaviour of concrete using damage models, Materials and Structures, 30 (1997), 349-354.
[27] J. Mazars and G. Pijaudier-Cabot, Continuum damage theory – application to concrete, J.

Eng. Mech-ASCE, 115 (1989), 345-365.
[28] E. Papa and A. Taliercio, Anisotropic Damage Model for the Multiaxial Static and Fatigue Behaviour of Plain Concrete, Eng. Fract. Mech, Vol. 55, No. 2 (1996), 163-179.
[29] C. R. Pedersen, Combined heat and moisture transfer in exposed building constructions. PhD Thesis, Technical University of Denmark, Lingby (1990).
[30] S. Pietruszczak and Z. Mróz, Finite element analysis of deformation of strain-softening materials, Int. J. Numer. Meth. Eng, 17 (1981), 327-334.
[31] A. Quarteroni and A. Valli, Domain Decomposition Methods for Partial Differential Equations, Oxford University Press Inc., New York, USA, 1999.
[32] SIFEL – Simple Finite Elements, `http://mech.fsv.cvut.cz/~sifel/index.html`,
[33] J. Skrzypek and A. Ganczarski, Modeling of Material Damage and Failure of Structures, Springer-Verlag Berlin Heidelberg, Germany, 1999.
[34] B. Smith, P. Bjørstad and W. Gropp, Domain Decomposition. Parallel Multilevel Methods for Elliptic Partial Differential Equations, Cambridge University Press, Cambridge, UK, 1996.
[35] V. Šmilauer and T. Krejčí, Multiscale Model for Temperature Distribution in Hydrating Concrete, International Journal for Multiscale Computational Engineering, Vol. 7, N. 2 (2009), 135-151.
[36] P. Šolín, J. Červený and I. Doležel, Arbitrary-level hanging nodes and automatic adaptivity in the hp-FEM, Math. Comput. Simulat, Vol. 77, Iss. 1 (2008), 117-132.
[37] P. Šolín, L. Dubcová and J. Kruis, Adaptive hp-FEM with dynamical meshes for transient heat and moisture transfer problems, J. Comput. Appl. Math, Vol. 233, Iss. 12 (2010), 3103-3112.
[38] P. Štemberk and P. Kalafutová, Modeling very early age concrete under uniaxial short-time and sustained loading, Mechanika, Vol. 70, N. 2 (2008), 16-21.
[39] T3D – automatic mesh generator, `http://mech.fsv.cvut.cz/~dr/t3d.html`,
[40] A. Toselli, and O. Widlund, Domain Decomposition Methods – Algorithms and Theory, Springer-Verlag, Berlin, Germany, 2005.